

# Spatial Distributions of Inelastic Events Produced by Electrons in Gaseous and Liquid Water<sup>1,2</sup>

H. G. PARETZKE,\* J. E. TURNER,† R. N. HAMM,† R. H. RITCHIE,† AND H. A. WRIGHT†<sup>3</sup>

\*GSF-Institut für Strahlenschutz, D-8042 Neuherberg, Federal Republic of Germany; and †Health and Safety Research Division, Oak Ridge National Laboratory, Oak Ridge, Tennessee 37831-6123

PARETZKE, H. G., TURNER, J. E., HAMM, R. N., RITCHIE, R. H., AND WRIGHT, H. A. Spatial Distributions of Inelastic Events Produced by Electrons in Gaseous and Liquid Water. *Radiat. Res.* 127, 121-129 (1991).

The spatial distributions of ionizations and other inelastic events in charged-particle tracks are important quantities that influence the final outcome of radiation interaction. Calculations of such distributions are presented for the tracks of electrons in the energy range 100 eV to 10 keV in liquid water and water vapor, and the results are compared. The distributions include the frequency of nearest-neighbor distances for all inelastic events, the mean nearest-neighbor distances for ionizations and for all inelastic events as a function of electron energy, the frequency of distances between all ionizations and all inelastic events, and the farthest distances between all inelastic events in electron tracks. The physical differences between liquid water and water vapor are discussed in terms of the respective inverse mean free paths, the collision spectra, and the nonlocalization of energy losses that are likely to occur in the liquid. © 1991

Academic Press, Inc.

## INTRODUCTION

Understanding the basic mechanisms of radiation damage to biological systems continues to be a significant problem. It has become increasingly clear that sensitive biological targets on the order of nanometers in size (e.g., the DNA molecule) play an important role in the production of biological effects. Consequently, spatial correlations of chemical changes produced by a charged particle within distances of the order of nanometers are important for determining

<sup>1</sup> Research sponsored in part by the Office of Health and Environmental Research, U.S. Department of Energy, under Contract DE-AC05-84OR21400 with Martin Marietta Energy Systems, Inc., and by the Commission of the European Communities, DG XII, under Contract BI-6-0011-D.

<sup>2</sup> The U.S. Government's right to retain a nonexclusive royalty-free license in and to the copyright covering this paper, for governmental purposes, is acknowledged.

<sup>3</sup> Present address: Consultec, Inc., Pellissippi Center, Suite 110, 725 Pellissippi Parkway, Knoxville, TN 37932-3300.

the response of biological systems to ionizing radiation (1, 2).

Measurements of the interaction of a charged particle with an isolated molecule can be made in the gas phase, and a number of such experiments have been carried out. However, interaction with a molecule in the liquid is also influenced by its neighbors, and the molecule does not always act individually. Indeed, when a charged particle traverses liquid water, some of its energy might be imparted to a quantized collective state (plasmon), which may involve the coherent oscillation of  $\sim 10^9$  electrons (3). The plasmon can subsequently decay by a specific localized transition, which can produce an excited or ionized water molecule nanometers away from the location of the corresponding energy-loss event of the incident particle. Other differences also characterize the liquid phase. For example, the ionization threshold, which is 12.6 eV in water vapor (4), may be as low as 8 eV in the liquid (3). The liquid also has a lower value for the average energy required to produce an ion pair (about 20 eV/ip), compared with the measured and calculated value of about  $W = 30$  eV/ip for the vapor at high electron energies.

For studying the effect of phase differences on charged-particle tracks in water, we have used the Monte Carlo computer code, MOCA-8, developed at GSF for calculations of the transport of electrons in the vapor (5) and the Monte Carlo computer code, OREC, developed at ORNL for calculations in the liquid (6). In earlier publications (7-9), we have discussed the physical bases for the two different computer codes and have compared various aspects of energy deposition, yields, and fluctuations that occur in the two phases at unit density. Kaplan *et al.* have also made independent studies to compare liquid water and water vapor in their calculation of primary product yields (10). The present paper addresses differences in the spatial patterns of energy deposition and ionization.

Spatial correlations of ionizations and other inelastic events over the nanometer distance range are of interest for several reasons. First, they determine the initial spatial relationships of the active chemical species produced in an irradiated system, which are important for determining the

subsequent chemical interactions that occur within a charged-particle track (11, 12). When the particle interacts with liquid water, it produces ionizations and excitations within a very short time ( $\sim 10^{-15}$  s in local regions of its path). These initial disturbances result in the production of reactive chemical species, such as OH and H radicals,  $\text{H}_3\text{O}^+$  ions, and hydrated electrons, by  $\sim 10^{-12}$  s. The species then diffuse and interact with one another or with other molecules that are present (13–15). These chemical reactions, which occur stochastically, are strongly dependent on the spatial distribution of the initial events in the track (11, 12, 16, 17). Second, biological systems are often able to repair certain kinds of damage produced in isolated events. However, multiple damage sites within close proximity of each other might lead to damage that cannot be repaired completely or that might be misrepaired, thus leading to permanent changes in the system.

In this paper we first review the main underlying physical quantities, i.e., the inelastic inverse mean free paths, or macroscopic cross sections, for both ionizations and all inelastic events for water in its liquid and vapor phases. We also discuss the nonlocalization function that is used to describe the spatial effects associated with the assumed collective excitation and decay in the liquid. We then present and compare the results of several calculations made for water in the two phases. These include nearest-neighbor distributions, distance distributions for all inelastic events, and distributions of “farthest” events in electron tracks. The paper focuses on electrons having initial energies in the range 100 eV to 10 keV.

#### COMPARISON OF PHYSICAL DATA FOR LIQUID AND VAPOR PHASES

Reference (7) gives a detailed description of the physical differences represented in the two Monte Carlo codes, MOCA-8 and OREC, for water vapor and for liquid water. The two features that have a direct effect on the spatial distributions of inelastic events are the respective inverse mean free paths and the nonlocalization of energy losses that takes place exclusively in the liquid. We discuss these two aspects of the calculations in this section.

The inverse mean free paths (IMFP), or macroscopic cross sections, for ionization and total inelastic scattering for electrons in water in the liquid and vapor phases at unit density are shown as functions of energy in Fig. 1. The inverse mean free path for excitation (not shown) is the difference between the total and the ionization inverse mean free paths. The ionization inverse mean free paths are very similar above 300 eV. Above about 40 eV, the ionization inverse mean free path is larger in the liquid; at lower energies the situation is reversed. The mass stopping powers of the two phases are very similar at all energies (9, 18). Figure 1 shows that the relative portion of energy loss in excitations and ionizations is considerably different in the two phases. The effect of these differences, coupled with the

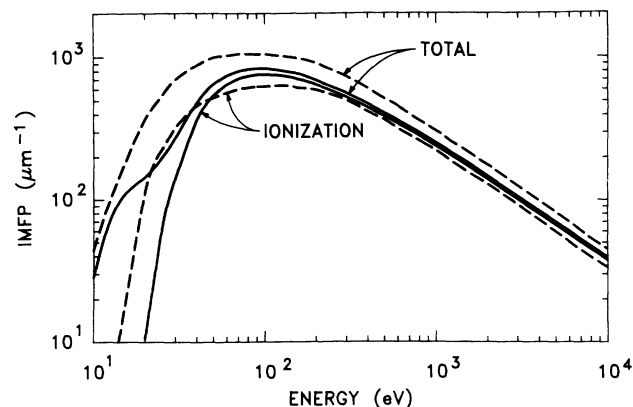


FIG. 1. Inverse mean free paths (IMFP), or macroscopic cross sections, for ionization and total inelastic scattering for electrons in water in the liquid (—) and vapor (---) phases.

generally “harder” single-collision spectrum for the liquid (7), results in the lower  $W$  value found for the liquid. The relative yields of excitations and ionizations determine the relative yields of the different reactive chemical species (H, OH, hydrated electron, and  $\text{H}_3\text{O}^+$ ) in an electron track at  $10^{-12}$  s, when diffusion-controlled, intratrack chemical reactions start to take place (16, 17).

As mentioned already, energy transferred to the liquid from an electron can be shared collectively by a large number of electrons. This subject has been reviewed recently by Ritchie *et al.* (19). Collective excitations in the condensed medium are assumed to be centered about the path of the electron and to relax through several channels for single- and many-particle decay. The probabilities for different modes of decay are taken to be proportional to the imaginary parts of the respective partial dielectric functions and to depend on the lateral distance  $b$  from the track. As derived in the Appendix, we use the following probability  $P(b)db$  for interaction at a lateral distance between  $b$  and  $b + db$  from an electron track (6, 19):

$$P(b)db = C \frac{e^{-\omega b/v\gamma} b db}{b_0^2 + b^2}.$$

Here  $\hbar\omega$  is the energy loss,  $v$  is the electron speed,  $\gamma = 5$  and  $b_0 = 0.2$  nm are constants, and  $C$  is a normalization factor. We assume that collective excitations are limited to energy losses  $\hbar\omega < 50$  eV and to lateral displacements  $b < 10$  nm. When such an excitation occurs in the computer simulation, a distance is selected from the distribution  $P(b)$  and a point of interaction is chosen in a random azimuthal direction at a point displaced laterally by this distance from the electron’s path.

The effect of the nonlocalization algorithm is shown in Fig. 2 for electron energies of 100 eV and 1 and 10 keV. (For the vapor, the corresponding distribution is a  $\delta$ -function at  $b = 0$  for all energies.) At 100 eV, an average of about

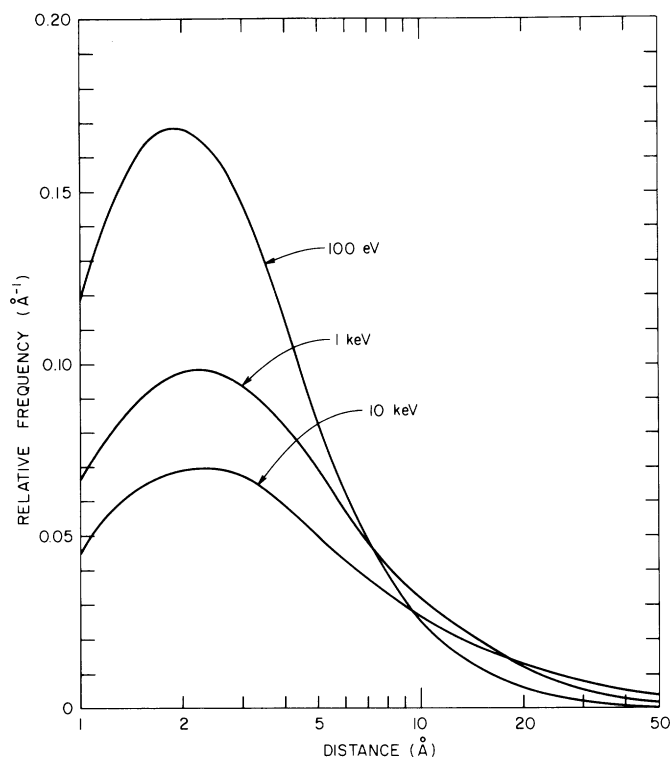


FIG. 2. The relative frequency  $P(b)$  for the lateral nonlocalization distances from the paths of 100-eV and 1- and 10-keV electrons in liquid water. Only events involving energy transfers of less than 50 eV are treated as nonlocal.

96% of the inelastic collisions of an electron involve nonlocal energy losses; at 500 eV and above, the corresponding figure is 80%. When a 100-eV electron and all of its secondaries are slowed down completely, nonlocal energy-loss events constitute over 99% of the total. For a stopping electron of energy  $\geq 500$  eV and all of its secondaries, about 94% of all inelastic collisions are nonlocal.

### DISTANCE MATRICES

Basic information about the spatial aspects of inelastic collisions within a complete electron track is contained in the "distance" matrix, defined in the following manner. All inelastic events for an electron and all of its secondaries, transported to subexcitation energies, are numbered 1, 2, 3,  $\dots$ ,  $n$  in an arbitrary order (e.g., the order in which they occur in the calculations), where  $n$  is their total number. The matrix is constructed with elements  $r_{ij}$ , giving the distances between all pairs of events  $i$  and  $j$ . The matrix is thus symmetric with rank  $n$  and has diagonal elements of zero ( $r_{ii} = 0$ ).

An example of a 100-eV electron track in liquid water is shown in Fig. 3a, where each dot represents the location of an inelastic event, projected into the plane of the page. This particular track contains a total of  $n = 9$  such events for the initial electron and its secondaries. The original electron

started at the origin ( $x = y = z = 0$ ), traveling in the direction of the positive  $x$  axis with an initial energy of 100 eV. After a number of elastic scatterings, the electron experienced its first inelastic collision—an ionizing event at the location  $i = 1$ . After nine inelastic events, all electrons have subexcitation energies, i.e., energies below the assumed threshold of 7.4 eV for electronic transitions in liquid water.

The distance matrix in Fig. 3b is calculated for the track in Fig. 3a. It illustrates the basis for computing a number of distribution functions presented in subsequent figures. For example, the distribution of nearest-neighbor distances for the nine event locations can be read from the matrix. These nearest-neighbor distances are, for  $i, j = 1, 2, \dots, 9$ , as follows:  $r_{12} = 1.6$ ,  $r_{24} = 0.7$ ,  $r_{31} = 1.9$ ,  $r_{42} = 0.7$ ,  $r_{56} = 0.7$ ,  $r_{65} = 0.7$ ,  $r_{79} = 1.2$ ,  $r_{89} = 0.9$ , and  $r_{98} = 0.9$  nm. By making computations for a large number of tracks, one can derive the mean frequency distribution for the nearest-neighbor distances for inelastic events, the mean distance of nearest neighbors, etc.

Alternatively, one can calculate distance matrices for certain excitations or ionization events alone. Some of the analyses below are carried out separately for different inelastic events.

### SOME DISTRIBUTIONS FOR SIMPLIFIED TRACKS

Before presenting our findings for actual electron tracks, it is instructive to consider some nearest-neighbor distributions computed for a few idealized, artificial tracks.

First, we consider a particle that continually travels along a straight line and has an inelastic collision every time it moves a given distance  $z_0$  along that line (no elastic scattering). In this case of equidistant collisions along a straight line, the nearest-neighbor distribution function for inelastic collisions is a  $\delta$ -function at  $z = z_0$ , the distance between collisions. If, instead of the nearest-neighbor distribution, one plots its complementary cumulative distribution function, i.e., the relative number of inelastic collisions that have their nearest neighbor at a distance greater than  $z$ , then one obtains the step-function curve, labeled (1) in Fig. 4, for the relative distance  $z/z_0$ .

Second, we treat equidistant inelastic scattering events again (event separation  $z_0$ ), but with an isotropic change in direction (in three dimensions) each time the scattering occurs (no elastic scattering). The resultant distribution is curve (2) in Fig. 4. In this case, the tracks can "bend back" on themselves and produce events closer together than  $z_0$ , as seen in curve (2) where the function drops below the previous step function. Since the nearest neighbor is never more than a distance  $z_0$  away, the distribution function is again zero for  $z > z_0$ .

It is interesting to note that curve (2) has the computed value 0.24 at  $z = z_0$ . For the site of a third collision to be a distance  $z_0$  from the first, the line between the second and third must make an angle of  $60^\circ$  with the line connecting

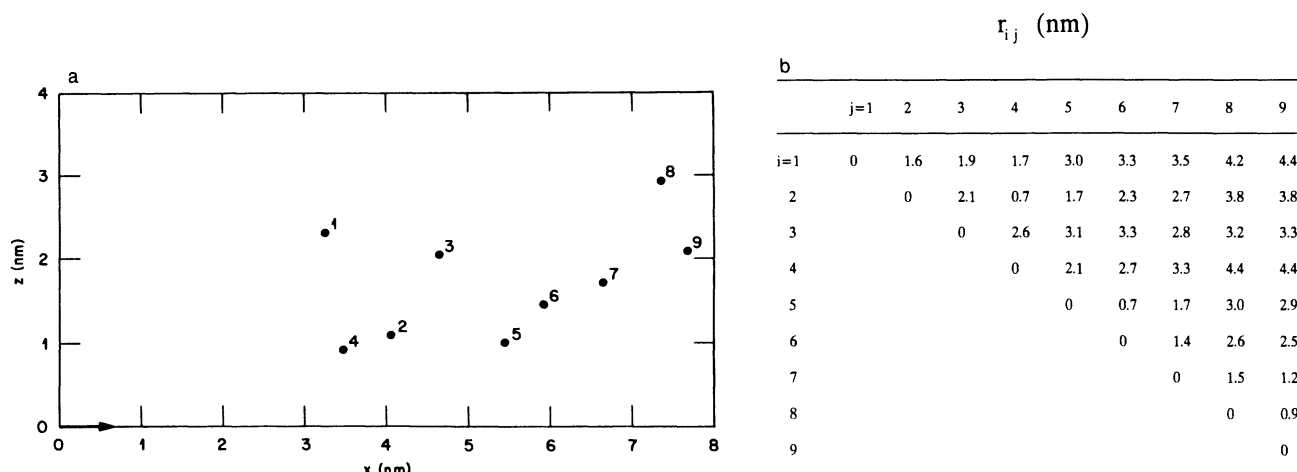


FIG. 3. (a) Example of a complete 100-eV electron track with its secondary electrons. Each dot represents the position, projected into the  $xz$  plane of the figure, of one of nine inelastic events experienced by the primary or a secondary electron. The original electron started at the origin in the direction of the positive  $x$  axis, as shown by the arrow. (b) Distance matrix for all pairs of inelastic events in the 100-eV electron track shown in Fig. 3(a).

the first and second. The three sites then form an equilateral triangle. Rotation of this triangle about the line connecting the first two collisions gives a right circular cone, within which any third event will be no farther away than  $z_0$  from the first. The  $120^\circ$  of the cone sweeps out exactly one-fourth of the total  $4\pi$ -steradian solid angle available for the third collision. Thus the value 0.24 at  $z = z_0$  calculated here (with 100 collisions per track) is very close to the theoretical value 0.25 for a track with only three inelastic events.

Case (3) in Fig. 4 shows an example of a straight-line path with a constant inelastic scattering cross section, i.e., an

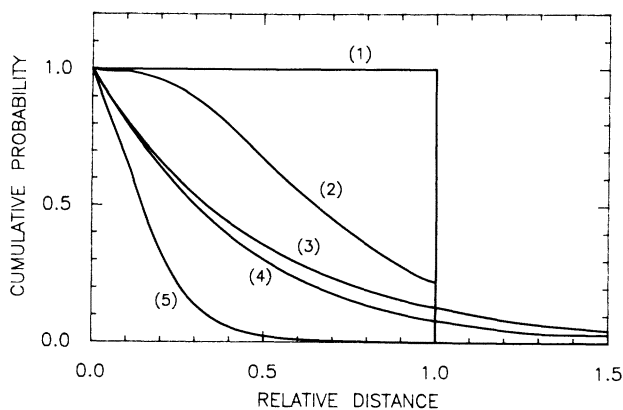


FIG. 4. Probability that nearest neighbors for inelastic events are at a relative distance greater than  $z/z_0$ , calculated for the conditions described in text: (1) straight line, constant distance  $z_0$  between inelastic collisions, no angular scattering; (2) equidistant inelastic collision distance  $z_0$ , but with isotropic scattering each time, no elastic scattering; (3) straight line with random exponentially distributed flight distances (macroscopic cross section  $\mu = 1/z_0$ ), no angular scattering; (4) random exponentially distributed flight distances ( $\mu = 1/z_0$ ) with isotropic inelastic scattering, no elastic scattering; (5) same as (4) with a random number (average = 9) of isotropic elastic scatterings between inelastic events.

exponential probability of traveling a given distance  $z$  between inelastic collisions. The inelastic mean free path is  $z_0$ , corresponding to a macroscopic cross section  $\mu = 1/z_0$ . Case (4) is the same as (3), except that an isotropic change in the direction of travel is selected at each collision (no elastic scattering). As seen from the figure, this angular scattering apparently has only a small additional effect on the cumulative distribution.

Frequent isotropic elastic scattering tends to make the motion of electrons more diffusive in nature, with a resulting shift of nearest neighbors for inelastic events to shorter separations. We superimposed stochastically on the conditions used to obtain curve (4) an average of nine isotropic "elastic" scattering events between every inelastic collision. The resultant distribution is shown as curve (5) in Fig. 4. Comparison of curves (4) and (5) shows the effect of elastic scattering in this example in bringing the nearest inelastic events closer together.

Figure 5 shows the frequency distributions for the five cumulative plots in Fig. 4. The frequency for case (1) is a  $\delta$ -function at unity, the only possible nearest-neighbor distance. Case (2), which permits distances less than unity, also gives a  $\delta$ -function at unity, the maximum possible nearest-neighbor separation.

#### NEAREST-NEIGHBOR DISTANCE DISTRIBUTIONS

The procedure described in the section on distance matrices was carried out to calculate the nearest-neighbor distributions for all inelastic events in electron tracks in liquid water and in water vapor at unit density. The results for electrons of initial energies of 100 eV and 1 keV are shown in Fig. 6, where the frequency distributions for nearest neighbors are plotted as functions of distance. The curves

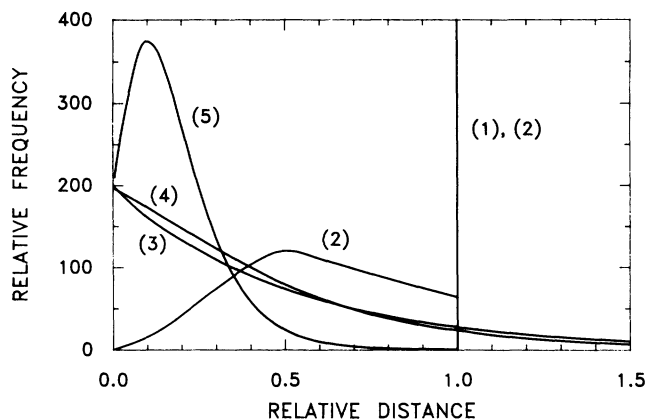


FIG. 5. Differential relative frequency distributions for the five cumulative plots shown in Fig. 4.

for 10-keV electrons, not shown, are close to those for 1 keV. The most probable nearest-neighbor distance is about 0.6 nm in the liquid, compared with about 0.1 to 0.2 nm in the vapor. This difference is due mainly to the assumption of collective states in liquid water.

The effect of the nonlocalization of energy absorption in the condensed phase for 100-eV electrons is shown by the curve marked NN, which was computed with the nonlocalization algorithm "turned off." While this distribution is shifted to shorter distances relative to the other liquid curve for 100 eV, it is still relatively far from the corresponding curve for the vapor. The remaining difference is due mainly to the longer mean free path in the liquid between subsequent collisions (see Fig. 1).

Figure 7 shows the mean distance between nearest neighbors for ionizations and for all inelastic events in the tracks of electrons of given initial energies in liquid water and

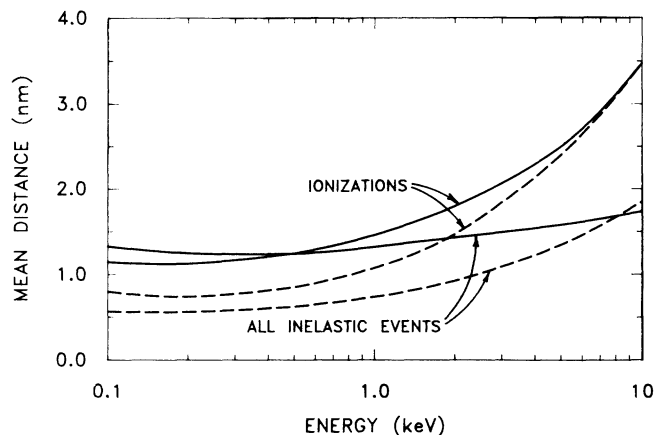


FIG. 7. Mean distance between next neighbors for ionizations and for all inelastic events in the tracks of electrons of different initial energies in water in the liquid (—) and vapor (---) phases.

water vapor. This average is but one measure of the compactness of charged-particle tracks. It is seen that these mean next-neighbor distances are larger in the liquid at electron energies below about 10 keV, where they are comparable. This finding reflects the nonlocalization of energy losses in the liquid. The moderate energy dependence at the lower energies reflects the highly diffusive but compact spatial character of the electron tracks. At higher energies, the mean values increase, the relative change being larger for the vapor. This behavior probably reflects the harder collision spectrum for electron energy losses in the liquid at these initial electron energies. As seen in a comparison of the slowing-down spectra (7), the initial energy of the primary electrons is less rapidly degraded in the vapor, resulting in tracks that are somewhat less compact on a larger scale.

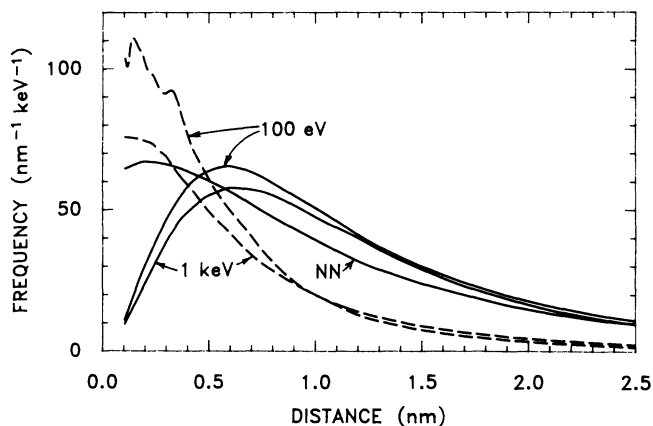


FIG. 6. Nearest-neighbor distributions for all inelastic events for tracks of electrons with initial energies of 100 eV and 1 keV in liquid water (—) and water vapor (---); curve labeled NN ("no nonlocalization") is the distribution for the liquid at 100 eV with the nonlocalization of energy transfer turned off in the calculations.

## DISTRIBUTIONS FOR ALL EVENTS

We next compare the frequency distributions for all inelastic events and for ionizations in liquid water and water vapor. These are plotted in Figs. 8 and 9 for electrons with initial energies of 100 eV and 1 keV. As with the nearest-neighbor distributions in Fig. 6, nonlocalization of energy losses and the harder collision spectrum in the liquid greatly reduce the probability that any pair of events occur at a separation of less than several tenths of a nanometer. In contrast, such separations (at unit density) are common in the vapor. As mentioned above, subsequent chemical reactions that occur in irradiated media are strongly dependent on these initial distributions (11, 12, 16, 17). Figures 8 and 9 clearly bring out the expectation that significant differences are to be expected between calculations of the later chemical evolution in a track, depending on whether track-

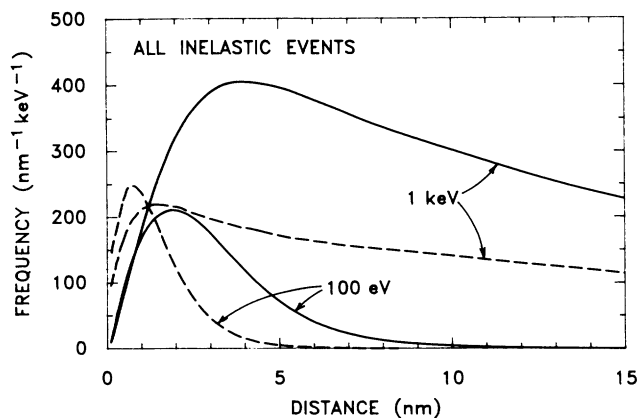


FIG. 8. Distance distributions for all inelastic events in tracks of 100-eV and 1-keV electrons in water in the liquid (—) and vapor (---) phases.

structure results for the liquid or the vapor are used as input.

#### FARTHEST DISTANCES BETWEEN EVENTS

It is also of interest to consider the distribution of farthest distances between any two inelastic events in electron tracks (as another measure of track compactness). Calculations at 100 and 500 eV show that the electron tracks in the liquid are considerably more spread out than in the vapor, again due mainly to the nonlocalization of energy losses and the harder collision spectrum in the liquid. At 1 keV, there is no great difference in the distribution of farthest distances; for 5 keV and higher energies, tracks in the vapor are characterized by larger values of the farthest distances.

Figure 10 gives the farthest distance that is exceeded by 5 and 50% of the electron tracks at a given energy in the liquid and vapor. At energies  $\leq 700$  eV the liquid curves lie above those for the vapor, then the curves cross, and the distances are somewhat larger for water vapor. At higher energies, the

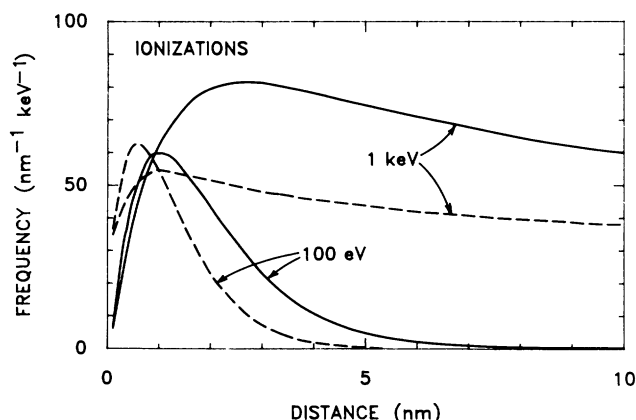


FIG. 9. Distance distributions for all ionizations in tracks of 100-eV and 1-keV electrons in water in the liquid (—) and vapor (---) phases.

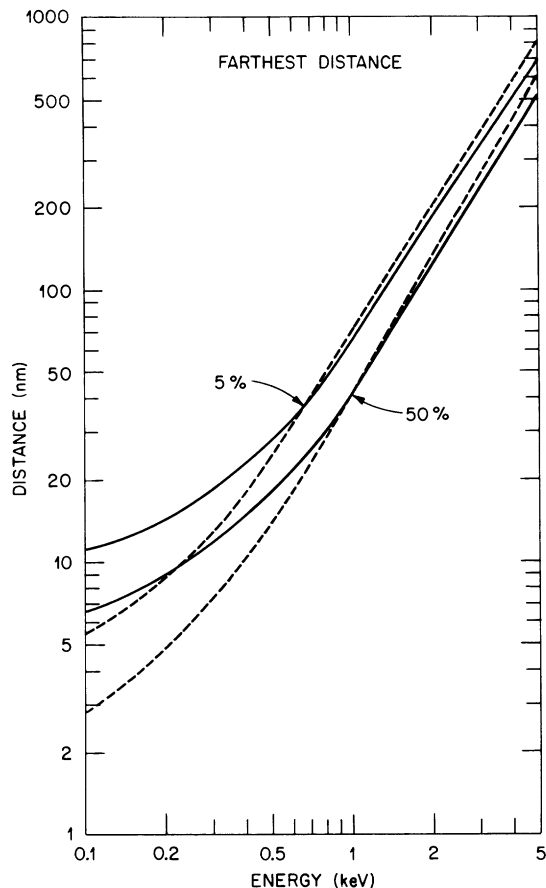


FIG. 10. Farthest distances exceeded by 5 and 50% of the tracks of electrons as a function of their initial energy in liquid water (—) and water vapor (---).

distance exceeded by 5% of the tracks becomes comparable to the csda range.

#### SUMMARY

In this study we have compared results of Monte Carlo computations carried out for water in its vapor and liquid phases, with particular emphasis on the spatial distributions of inelastic events. The assumed nonlocalization of energy-absorption events in the liquid, differences in the mean free paths, and the harder collision spectrum are found to have pronounced effects in "separating" neighboring events out to distances of several nanometers, compared with the vapor. In addition, the liquid is characterized by a larger cross section for ionization. These effects in the condensed phase can be expected to play an important role in subsequent intratrack chemistry and in producing different types of indirect and direct biological damage.

#### APPENDIX

The localization of initially unlocalized excitations in a water medium is far from being well understood. Experi-

ment furnishes little guidance about the details of this process in complex molecular liquids. Nevertheless, we feel justified in adopting a simple approach to estimate its effects in irradiated water. As originally implemented in OREC, the localization mechanism was modeled using a collective picture to describe excitations created by charged particles. The basis of this model can be described as follows.

Assume that the swift charged particle has charge  $Ze$  and mass  $M$  and proceeds through the condensed matter medium with speed  $\nu$ . The interaction Hamiltonian between the particle and collective modes in the system can be taken as

$$H_{ep} = Z \sum_{\mathbf{q}} \alpha_{\mathbf{q}} e^{i\mathbf{q}\cdot\mathbf{r}} (b_{\mathbf{q}} + b_{-\mathbf{q}}^{\dagger}), \quad (\text{A1})$$

where  $b_{\mathbf{q}}$  is a destruction operator for a collective excitation with wave vector  $\mathbf{q}$ , and the coupling constant is

$$\alpha_{\mathbf{q}}^2 = \frac{2\pi\hbar e^2\omega_p^2}{\Omega\omega_{\mathbf{q}}q^2}. \quad (\text{A2})$$

Here,  $\Omega$  is the normalization volume,  $\omega_p$  is the plasma frequency of the electronic system, and the eigenfrequency of a plasmon with wave number  $q$  is

$$\omega_{\mathbf{q}} = \sqrt{\omega_p^2 + \beta^2 q^2 + \frac{\hbar^2}{4M^2} q^4}, \quad (\text{A3})$$

where  $\beta$  is the speed at which disturbances propagate in the valence electron gas. The  $q^2$  term has its origin in the dispersion of electrons in the medium and the term containing  $q^4$  represents quantal recoil of the electrons.

To proceed with the theory, assume that the state vector of the initial state may be written

$$|i\rangle = \frac{e^{i\mathbf{p}_i\cdot\mathbf{r}}}{\sqrt{\Omega}} |O\rangle \quad (\text{A4})$$

and that the final state vector may be expressed as

$$|f\rangle = \frac{e^{i\mathbf{p}_f\cdot\mathbf{r}}}{\sqrt{\Omega}} b_{\mathbf{q}}^{\dagger} |O\rangle, \quad (\text{A5})$$

where  $|O\rangle$  is the vacuum state of the collective-mode field.

First-order Golden Rule perturbation theory gives for the inverse mean free path,  $\Lambda^{-1}$  for plasmon creation,

$$\Lambda^{-1} = \frac{2\pi}{\nu} \sum_{\mathbf{p}_f} \sum_{\mathbf{q}} |\langle f | H_{ep} | i \rangle|^2 \delta(\epsilon_{\mathbf{p}_f} - \epsilon_{\mathbf{p}_i} - \omega_{\mathbf{q}}), \quad (\text{A6})$$

where  $\epsilon_{\mathbf{p}} = \mathbf{p}^2/2M$  and we use atomic units henceforth. Evaluating the sum over  $\mathbf{p}_f$  one finds

$$\Lambda^{-1} = \frac{2\pi Z^2}{\nu} \sum_{\mathbf{q}} \alpha_{\mathbf{q}}^2 \delta(\nu \cdot \mathbf{q} - \frac{q^2}{2M} - \omega_{\mathbf{q}}), \quad (\text{A7})$$

where  $\nu = p_i/M$  in atomic units. For simplicity and to obtain an analytical form for the radial distribution, take  $\omega_{\mathbf{q}} \approx \omega_p$ . Then converting the sums to integrals as  $\Omega \rightarrow \infty$ , neglecting the second term in the energy-conserving  $\delta$ -function, and resolving the vector  $q$  as

$$\mathbf{q} = \mathbf{Q} + q_z \left( \frac{\nu}{\nu} \right), \quad (\text{A8})$$

where the  $\mathbf{Q}$  is perpendicular to  $\nu$ , we find

$$\Lambda^{-1} = \frac{Z^2\omega_p}{2\pi\nu^2} \int \frac{d^2Q}{Q^2 + \omega_p^2/\nu^2}. \quad (\text{A9})$$

This equation may be written in the equivalent form

$$\Lambda^{-1} = \frac{Z^2\omega_p}{2\pi\nu^2} \int \frac{d^2Q}{\sqrt{Q^2 + \omega_p^2/\nu^2}} \times \int \frac{d^2Q'}{\sqrt{Q'^2 + \omega_p^2/\nu^2}} \delta^2(\mathbf{Q} - \mathbf{Q}'), \quad (\text{A10})$$

or, using the identity  $\delta^2(\mathbf{Q} - \mathbf{Q}') = \int d^2b e^{i\mathbf{b}\cdot(\mathbf{Q}-\mathbf{Q}')}/(2\pi)^2$ , one has

$$\Lambda^{-1} = \frac{Z^2\omega_p}{8\pi^3\nu^2} \int d^2b \int \frac{d^2Q e^{i\mathbf{Q}\cdot\mathbf{b}}}{\sqrt{Q^2 + \omega_p^2/\nu^2}} \times \int \frac{d^2Q' e^{-i\mathbf{Q}'\cdot\mathbf{b}}}{\sqrt{Q'^2 + \omega_p^2/\nu^2}}. \quad (\text{A11})$$

Then

$$\Lambda^{-1} = \frac{Z^2\omega_p}{8\pi^3\nu^2} \int d^2b \left| \int \frac{d^2Q e^{i\mathbf{Q}\cdot\mathbf{b}}}{\sqrt{Q^2 + \omega_p^2/\nu^2}} \right|^2. \quad (\text{A12})$$

The integral over  $Q$  may be evaluated in terms of elementary functions. We assert that one may regard the integrand of the  $b$  integration as a differential inverse mean free path for interaction with the medium in the impact parameter variable  $b$  per unit volume in impact parameter space; then one writes

$$\frac{d^2\Lambda^{-1}}{d^2b} = \frac{Z^2\omega_p}{2\pi\nu^2} \left[ \frac{e^{-2\omega_p b/\nu}}{b^2} \right] \quad (\text{A13})$$

for the differential inverse mean free path in the two-dimensional parameter space. A more accurate result that does not diverge as  $b \rightarrow 0$  would be found by retaining the full  $q$  dependence of  $\omega_{\mathbf{q}}$ . One can show that  $d^2\Lambda^{-1}/d^2b$  di-

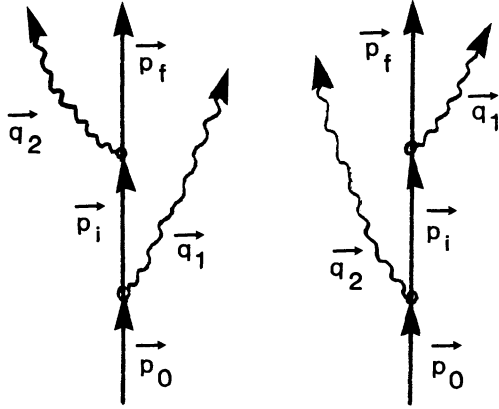


FIGURE 11

verges only logarithmically as  $b \rightarrow 0$  and that  $\Lambda^{-1}$  is thus finite, as it must be. A more accurate expression is

$$\frac{d^2 \Lambda^{-1}}{d^2 b} = \frac{\pi Z^2 \omega_p^3}{16 \beta^2 \nu^2} I_0^2 \left( \frac{b \omega_-}{\beta} \right) K_0^2 \left( \frac{b \omega_+}{\beta} \right), \quad (\text{A14})$$

where  $\omega_{\pm} = (\omega_p / \sqrt{2}) \sqrt{1 \pm \sqrt{2} \beta / \nu}$  and  $I_0$  and  $K_0$  are modified Bessel functions of order 0. This expression is valid when  $\nu \gg \beta \approx 1$  a.u. and reduces to that given in Eq. (A13) when  $b \gg \nu / \omega_p$ . For purposes of orientation, we note that the screening length  $\nu / \omega_p$  is  $\sim 14$  nm for a 100-keV electron in water,  $\sim 1.4$  nm for a 1-keV electron and  $\sim 0.14$  nm for a 10-eV electron.

This approach may be extended to yield a differential inverse mean free path for the creation of two excitations in the medium by the swift charged particle. Figure 11 shows Feynman diagrams representing the lower-order interactions corresponding to this process.

Standard second-order perturbation theory gives the following expression for the inverse mean free path,  $\Lambda^{-1}$ ,

$$\begin{aligned} \Lambda^{-1} = & \frac{2\pi Z^2}{\nu \Omega^2} \sum_{\mathbf{q}_1} \sum_{\mathbf{q}_2} \sum_{\mathbf{p}_f} \left| \sum_{\mathbf{p}_i} \frac{\alpha_{q_1} \alpha_{q_2} \delta^3(\mathbf{p}_i - \mathbf{p}_f - \mathbf{q}_2) \delta^3(\mathbf{p}_0 - \mathbf{p}_i - \mathbf{q}_1)}{\epsilon_{\mathbf{p}_0} - \epsilon_{\mathbf{p}_i} - \omega_{\mathbf{q}_1} + i\gamma} \right. \\ & \left. + \sum_{\mathbf{p}_i} \frac{\alpha_{q_1} \alpha_{q_2} \delta^3(\mathbf{p}_i - \mathbf{p}_f - \mathbf{q}_1) \delta^3(\mathbf{p}_0 - \mathbf{p}_i - \mathbf{q}_2)}{\epsilon_{\mathbf{p}_0} - \epsilon_{\mathbf{p}_i} - \omega_{\mathbf{q}_2} + i\gamma} \right|^2 \\ & \times \delta(\epsilon_{\mathbf{p}_0} - \epsilon_{\mathbf{p}_f} - \omega_{\mathbf{q}_1} - \omega_{\mathbf{q}_2}). \quad (\text{A15}) \end{aligned}$$

Here  $\mathbf{p}_0$  is the wave vector of the particle in its initial state and  $\gamma$  is the damping rate of the collective state. Although the damping rate in general depends on the momentum of the state, we assume for simplicity that it is constant.

Simplifying Eq. (A15) with the aid of the Kronecker  $\delta$ 's and letting  $\Omega \rightarrow \infty$  we find

$$\begin{aligned} \Lambda^{-1} = & \frac{Z^2}{8\pi^3 \nu} \int d^3 q_1 \int d^3 q_2 \vartheta \\ & \times \delta(\nu_0 \cdot \mathbf{q}_1 + \nu_i \cdot \mathbf{q}_2 - \omega_{q_1} - \omega_{q_2}) |\Gamma_{\mathbf{q}_1, \mathbf{q}_2}|^2 \quad (\text{A16}) \end{aligned}$$

and

$$\Gamma_{\mathbf{q}_1, \mathbf{q}_2} = \frac{1}{\nu \cdot \mathbf{q}_1 - \omega_p + i\gamma} + \frac{1}{\nu \cdot \mathbf{q}_2 - \omega_p + i\gamma}. \quad (\text{A17})$$

In obtaining this expression dispersion of the collective mode ( $\omega_q \approx \omega_p$ ) and recoil of the charged particle have been neglected. Following a procedure similar to that used above and employing approximations appropriate to large values of the coordinates, one finds

$$\frac{d^5 \Lambda^{-1}}{d^2 b_1 d^2 b_2 dz} = \frac{4\pi^2 \omega_p^2 Z^2}{\nu^4} \frac{e^{-2\omega_p b_1 / \nu}}{b_1^2} \frac{e^{-2\omega_p b_2 / \nu}}{b_2^2} e^{-2\gamma |z| / \nu}. \quad (\text{A18})$$

This describes the probability of two interactions by the particle per unit path length in the medium per unit volume in impact parameter space for interaction 1, per unit volume in impact parameter space for interaction 2, and per unit separation,  $z$ , between the interactions. This result is neat and compact and seems quite in accord with intuition.

In work with OREC the above results have been used to model the localization of initially unlocalized excitations created by electrons or ions in water. For simplicity in representing the localization process in a Monte Carlo calculation, it was assumed that all energy losses in amounts less than  $\sim 50$  eV by swift electrons or ions were initially unlocalized and subsequently localized at radial separation  $r$  from the point at which the energy loss is found to occur in the Monte Carlo calculation. The distribution from which this radial distance is chosen is taken to be

$$P(b)db = C \frac{\exp(-\omega b / \nu \gamma)}{b_0^2 + b^2} b db. \quad (\text{A19})$$

Here  $\hbar\omega$  is the energy loss,  $\gamma$  is a constant of the order of unity,  $b_0$  is a constant  $\sim 0.1$  nm, and  $C$  is a normalization constant chosen such that  $\int_0^{b_{\max}} P(b)db = 1$ . In these calculations  $b_{\max}$  is chosen to be 10 nm. The constant  $\gamma$  is intended to represent, schematically, propagation of coherent excitations before localization as well as our lack of knowledge about the localization process in a complex molecular liquid such as water. It was taken equal to 5 to emphasize the radial extension of the localization process, and may be altered when relevant experimental data become available.

Recent experimental data have indicated that coherent excitations created by swift charged particles in metallic systems have a rather narrow radial extension about the path of the particle. Scanning transmission electron microscopy (STEM) experiments on plasmon losses in the vicinity of a metallic boundary show spatial resolution  $\sim 0.4$  nm when the quantity  $\nu/\omega$  appropriate to the experiments is quite large, i.e.,  $\sim 4$  nm (20). Similar high resolution is achieved in band gap spectroscopy of defects in semicon-

ductors (21). Recent work in STEM has shown that it is possible to obtain secondary electron signals with  $\sim 1$  nm spatial resolution and 1 eV energy resolution again when the parameter  $\nu/\omega$  corresponding to the experiments is  $\sim 4$  nm (22, 23). We have given theoretical justification for the high resolution observed for free-electron-like systems (19, 24, 25).

However, in view of the uncertainties in our knowledge of fundamental interactions in complex molecular liquids, and in view of the good agreement found (17) between calculations based in part on the OREC transport code and measurements from electron pulse radiolysis, we feel justified in retaining the presently implemented algorithm for representing localization of initially unlocalized excitations in water until additional data become available.

RECEIVED: January 18, 1990; ACCEPTED: February 9, 1991

## REFERENCES

1. J. F. WARD, DNA damage produced by ionizing radiation in mammalian cells: Identities, mechanisms of formation, and repairability. In *Progress in Nucleic Acid Research and Molecular Biology* (W. E. Cohn and K. Moldave, Eds.), Vol. 35, pp. 95–125. Academic Press, San Diego, CA, 1988.
2. D. T. GOODHEAD, Deductions from cellular studies of inactivation, mutagenesis, and transformation. In *Radiation Carcinogenesis: Epidemiology and Biological Significance* (J. D. Boice, Jr., and J. F. Fraumeni, Jr., Eds.). Raven Press, New York, 1984.
3. R. H. RITCHIE, R. N. HAMM, J. E. TURNER, and H. A. WRIGHT, The interaction of swift electrons with liquid water. In *Sixth Symposium on Microdosimetry* (J. Booz and H. G. Ebert, Eds.), pp. 345–354. Commission of the European Communities, Harwood, London, 1978.
4. G. D. ZEISS, W. J. MEATH, J. C. F. MACDONALD, and D. J. DAWSON, Dipole spectrum of water vapor and its relation to the energy loss of fast charged particles. *Radiat. Res.* **63**, 64–82 (1975).
5. H. G. PARETZKE, Radiation track structure theory. In *Kinetics of Nonhomogeneous Processes* (G. R. Freeman, Ed.), Chap. 3. Wiley, New York, 1987.
6. R. N. HAMM, J. E. TURNER, R. H. RITCHIE, and H. A. WRIGHT, Calculation of heavy-ion tracks in liquid water. *Radiat. Res.* **104**, S-20–S-26 (1985).
7. J. E. TURNER, H. G. PARETZKE, R. N. HAMM, H. A. WRIGHT, and R. H. RITCHIE, Comparative study of electron energy deposition and yields in water in the liquid and vapor phases. *Radiat. Res.* **92**, 47–60 (1981).
8. J. E. TURNER, H. G. PARETZKE, R. N. HAMM, H. A. WRIGHT, and R. H. RITCHIE, Comparison of electron transport calculations for water in the liquid and vapor phases. In *Radiation Protection, Proceedings of the 8th Symposium on Microdosimetry* (J. Booz and H. G. Ebert, Eds.). Commission of the European Communities, Luxembourg, 1983.
9. H. G. PARETZKE, J. E. TURNER, R. N. HAMM, H. A. WRIGHT, and R. H. RITCHIE, Calculated yields and fluctuations for electron degradation in liquid water and water vapor. *J. Chem. Phys.* **84**, 3182–3188 (1986).
10. I. G. KAPLAN, A. M. MITEREV, and V. YA. SUKHONOSOV, Comparative study of yields of primary products in tracks of fast electrons in liquid water and in water vapor. *Radiat. Phys. Chem.* **27**, 83–90 (1986).
11. S. M. PIMBLOTT, J. A. LAVERNE, A. MOZUMDER, and N. J. B. GREEN, Structure of electron tracks in water. 1. Distribution of energy deposition events. *J. Phys. Chem.* **94**, 488–495 (1990).
12. A. CHATTERJEE, J. L. MAGEE, and S. K. DEY, The role of homogeneous reactions in the radiolysis of water. *Radiat. Res.* **96**, 1–19 (1983).
13. C. D. JONAH, M. S. MATHESON, J. R. MILLER, and E. J. HART, Yield and decay of the hydrated electron from 100 ps to 3 ns. *J. Phys. Chem.* **80**, 1267–1270 (1976).
14. C. D. JONAH and J. R. MILLER, Yield and decay of the OH radical from 200 ps to 3 ns. *J. Phys. Chem.* **81**, 1974–1976 (1977).
15. C. N. TROMBORE, D. R. SHORT, J. E. FANNING, JR., and J. H. OLSON, Effects of pulse dose on hydrated electron decay kinetics in the pulse radiolysis of water. Computer modeling study. *J. Phys. Chem.* **82**, 2762–2767 (1978).
16. J. E. TURNER, J. L. MAGEE, H. A. WRIGHT, A. CHATTERJEE, R. N. HAMM, and R. H. RITCHIE, Physical and chemical development of electron tracks in liquid water. *Radiat. Res.* **96**, 437–449 (1983).
17. J. E. TURNER, R. N. HAMM, H. A. WRIGHT, R. H. RITCHIE, J. L. MAGEE, A. CHATTERJEE and W. E. BOLCH, Studies to link the basic radiation physics and chemistry of liquid water. *Radiat. Phys. Chem.* **32**, 503–510 (1988).
18. J. C. ASHLEY, Stopping power of liquid water for low-energy electrons. *Radiat. Res.* **89**, 25–31 (1982).
19. R. H. RITCHIE, R. N. HAMM, J. E. TURNER, H. A. WRIGHT, J. C. ASHLEY, and G. J. BASBAS, Physical aspects of charged particle track structure. *Int. J. Radiat. Instrum. Part D Nuclear Tracks Radiat. Meas.* **16**, 141–155 (1989).
20. M. SCHEINFELD, A. MURRAY, and M. ISAACSON, Electron energy loss spectroscopy across a metal–insulator interface. *Ultramicroscopy* **16**, 233–240 (1985).
21. P. E. BATSON, K. L. KAVANAUGH, J. M. WOODALL, and J. W. MAYER, Scattering near a single misfit location in a dielectric medium of randomly distributed metal particles. *Phys. Rev. Lett.* **57**, 2729–2732 (1986).
22. A. L. BLELOCH, A. HOWIE, R. H. MILNE, and M. G. WALLS, Elastic and inelastic scattering effects in reflection electron microscopy. *Ultramicroscopy* **29**, 175–182 (1989).
23. D. IMESON, R. H. MILNE, S. D. BERGER, and D. MCMULLAN, Secondary electron detection in the scanning transmission electron microscope. *Ultramicroscopy* **17**, 243–250 (1985).
24. R. H. RITCHIE, A. HOWIE, P. M. ECHENIQUE, G. J. BASBAS, T. L. FERRELL, and J. C. ASHLEY, Plasmon effects in STEM electron spectra. *Scanning Microsc. Suppl.* **4**, 45–56 (1990).
25. R. H. RITCHIE, R. N. HAMM, J. E. TURNER, and H. A. WRIGHT, Radiation interactions and energy transport in the condensed phase. In *Physical and Chemical Mechanisms in Molecular Radiation Biology* (W. Glass and M. Varma, Eds.), in press.